A Complex Fulleride Superstructure—Decoupling Cation Vacancy and Anion Orientational Ordering in $Ca_{3+x}C_{60}$ with Maximum Entropy Data Analysis

J. B. Claridge,*,† Y. Kubozono,‡ and M. J. Rosseinsky*,†

Department of Chemistry, The University of Liverpool, Liverpool, L69 7ZD, United Kingdom, and Department of Chemistry, Okayama University, Okayama 700-8530, Japan

Received March 26, 2002. Revised Manuscript Received January 2, 2003

The structure of the alkaline-earth fulleride $Ca_{3.01}C_{60}$ is refined using maximum entropy data analysis of synchrotron powder diffraction data. Despite the size and complexity of the structural problem, the fulleride anion orientations and the details of multiple occupancy of the octahedral interstitial sites in the fcc anion array are determined. The power of the maximum entropy technique in solving underdetermined problems in powder crystallography is thus demonstrated.

Introduction

The mechanism underlying superconductivity in fullerenes is unclear, despite intensive studies of the electron-doped alkali-metal (A) A_xC_{60} systems.[1,2] High superconducting transition temperatures are qualitatively associated with proximity to metal−insulator transitions, and the fullerides are perhaps the most striking example of this. Estimates of the one-electron bandwidth, *W*, and the on-site interelectron repulsion, *U*, indicate that the superconducting A_3C_{60} metals should lie in the $U > W$ localized region of the Mott−Hubbard model and therefore be insulating because the electrons are prevented from delocalizing by the repulsion.[3] Several models have been put forward to account for the observed metallic behavior. More sophisticated theoretical treatments indicate that the degeneracy of the t_{1u} LUMO of C_{60} enhances near-neighbor hopping sufficiently for the experimentally observed values of *U* and *W* to permit metallic behavior and make the A_3C_{60} systems strongly correlated and orbitally polarized metals.[4]

An alternative mechanism to suppress the Mott−Hubbard transition is for cation vacancies to produce sufficient deviation from the A_3C_{60} composition to introduce hole carriers into the half-filled t_{1u} band, making the fullerides doped Mott−Hubbard insulators and introducing clear parallels with the high T_c copper oxides which may be of relevance given the recent increase in T_c. Experiments indicate that such vacancies are located on the tetrahedral sites.[5] The study of fullerides with structures related to that of K_3C_{60} in which well-defined cation vacancies occur is thus of importance.

$Yb_{2.75}C_{60}$ is the best-characterized example of cation vacancy ordering in metal fullerides.[6] The familiar face-centered cubic fcc unit cell of K_3C_{60}, containing four C_{60}^{3-} anions describing four octahedral (O) and eight tetrahedral (T) interstitial cation sites, is doubled in all three directions due to the ordering of eight tetrahedral cation vacancies. The octahedral cations relax away from the site center positions along 3-fold axes of the octahedra toward vacant neighboring T sites (Figure 1a). The equivalence of the fulleride anions is also removed by the vacancy ordering (Figure 1b), and the anion orientations are determined by the need to optimize the number of cation-pentagon contacts. Subsequent investigations of $Sm_{2.75}C_{60}$ and $Eu_{2.75}C_{60}$ have confirmed the main features of this model, while preferring cubic $Pa\bar{3}$ to orthorhombic *Pbca* symmetry.[7,8] All structural investigations have dealt in a statistical manner with the octahedral site occupancy—cation displacement from the site center leads to a cube of eight equivalent positions, one of which is favored due to proximity to the 8 T vacancies and the others are assumed to have an equal and minor occupancy. Given the disordered metal clusters found occupying the metal sites in Na_xC_{60} ($6 < x < 11$),[9,10] accurate identification of the species occupying the O sites in these T-vacancy ordered phases has wider significance in fulleride structural chemistry. In the structural studies of

* Corresponding authors. E-mail: m.j.rosseinsky@liv.ac.uk; claridge@liv.ac.uk.
† The University of Liverpool.
‡ Okayama University.

(1) Dahlke, P.; Denning, M. S.; Henry, P. F.; Rosseinsky, M. J. *J. Am. Chem. Soc.* **2000**, *122*, 12352−12361.
(2) Rosseinsky, M. J. *Chem. Mater.* **1998**, *10*, 2665−2685.
(3) Lof, R. W.; Veenendaal, M. A. v.; Koopmans, B.; Jonkman, H. T.; Sawatzky, G. A. *Phys. Rev. Lett.* **1992**, *68*, 3924.
(4) Gunnarsson, O.; Koch, E.; Martin, R. M. *Phys. Rev. B* **1996**, *54*, R11026.
(5) Bendele, G. M.; Stephens, P. W.; Fischer, J. E. *Europhys. Lett.* **1998**, *41*, 553−558.
(6) Ozdas, E.; Kortan, A. R.; Kopylov, N.; Ramirez, A. P.; Siegrist, T.; Rabe, K. M.; Bair, H. E.; Schuppler, S.; Citrin, P. H. *Nature* **1995**, *375*, 126−129.
(7) Claves, D.; Ksari-Habiles, Y.; Chouteau, G.; Touzain, P. *Solid State Commun.* **1998**, *106*, 431−435.
(8) Claves, D.; Hamwi, A. *Solid State Commun.* **2000**, *113*, 357−362.
(9) Rosseinsky, M. J.; Murphy, D. W.; Fleming, R. M.; Tycko, R.; Ramirez, A. P.; Siegrist, T.; Dabbagh, G.; Barrett, S. E. *Nature* **1992**, *356*, 416−418.
(10) Yildirim, T.; Zhou, O.; Fischer, J. E.; Bykovetz, N.; Strongin, R. A.; Cichy, M. A.; Smith III, A. B. S.; Lin, C. L.; Jelinek, R. *Nature* **1992**, *360*, 569.

10.1021/cm020171y CCC: $25.00
Published on Web 04/11/2003

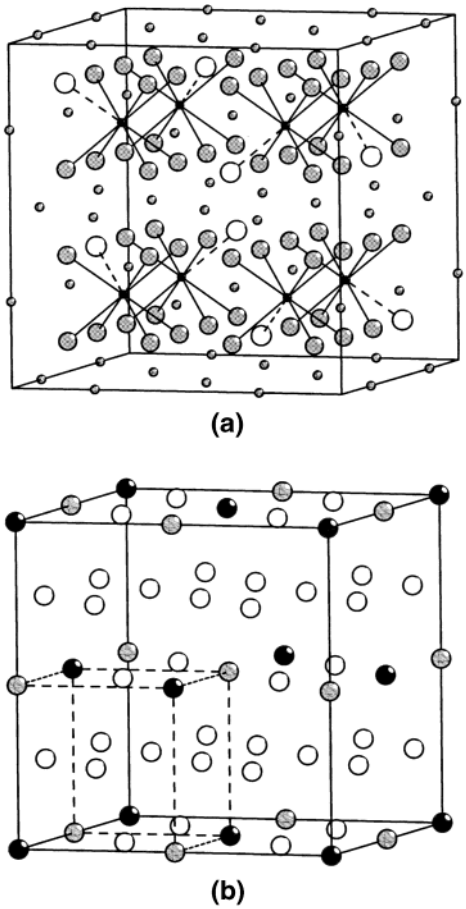

Figure 1. (a) The Ca_3C_{60} structure is based on doubling the fcc A_3C_{60} 14-Å unit cell in all three directions. The tetrahedral T cation sites within a subcell describe a cube, and the ordering of one vacancy per subcell produces the $Pa\bar{3}$ symmetry structure with a 28-Å unit cell shown in the figure. There are two distinct sets of octahedral (O) sites, distinguished by their relationship to the centers of the subcells and the arrangement of the T vacancies. The 8c sites (small black spheres) at the centers of the cubes of occupied T sites (within each subcell hatched large spheres) defined by the T vacancy (open large spheres, connected to the 8c site by a broken line) ordering and the 24d sites (gray, hatched small spheres) which do not lie on the 3-fold axes defined by the vacancy ordering. (b) The cation vacancy ordering generates three symmetry-inequivalent sets of fulleride anions: the 4a (black spheres) and 4b (gray, hatched) sets are constrained to lie on 3-fold axes passing through two diametrically opposed hexagonal faces of the anions whereas the remaining 24d anions (unshaded) are not orientationally constrained by symmetry.

$Sm_{2.75}C_{60}$ and $Eu_{2.75}C_{60}$, fulleride anion orientation was not considered, whereas in $Yb_{2.75}C_{60}$ the complex structural model was constructed by a remarkable series of model buildings and constrained Rietveld analyses.

Traditional Fourier synthesis methods of extracting electron densities from powder data suffer from two major problems. The first is the effect of termination due to unobserved peaks, which produce spurious features, making it difficult to extract physically meaningful residual electron density distribution maps. The other is due to the difficulty in obtaining accurate observed structure factors ($|F_{obs}|$), owing to the collapse of reciprocal space onto a one-dimensional diffraction pattern and the resulting partial or complete overlap of Bragg reflections. Both of these factors are significant for Ca_xC_{60} due to the large unit cell and lack of diffraction at high Q.

One method of overcoming this problem is the application of maximum entropy methods (MEM).[11−14] In this approach, rather than performing a Fourier transformation of the F_{obs} structure factors as obtained from the Rietveld refinement by apportioning the intensity of overlapping observed reflections according to the calculated structure factors, a density distribution is estimated and the information entropy is maximized within the errors of the observed data. Thus, MEM can be seen in some ways as the opposite of a Fourier synthesis, as an initial density is fitted to the observed scattering factors. (It is customary to start from an homogeneous density distribution.) As unobserved high Q peaks do not affect the density, accurate electron densities can be obtained from limited numbers of integrated intensities.[14] The detailed theory of MEM is covered in the above references. However, the use of MEM alone still maintains the F_{obs} as obtained from the initial extraction and is therefore biased toward the model used to extract the data. However, the results of an MEM calculation can be used to provide F_{calc} for a second extraction of F_{obs} from the observed data, which will be less biased toward the original model. Repeated extractions and MEM calculations should therefore yield the true scattering density. This cycling of the MEM results has been implemented by Izumi in RIETAN-2000, who has applied the so-called REMEDY cycles to a number of diffraction problems.[15,16]

We aim in this paper at a systematic evaluation of the occupied cation sites and preferred fulleride anion orientations by employing the model-independent maximum entropy method in combination with Rietveld analysis to develop a robust model for $Pa\bar{3}$ structure Ca_xC_{60}, without making assumptions over the symmetry constraints concerning anion orientation and cation site position and occupancy. The detailed structural analysis reveals a strong correlation between inter- and intrasite cation contacts, cation site occupancy, and anion orientational ordering and allows us to identify the specific cation sites occupied in this vacancy-ordered fulleride structure. Given the limitations inherent in powder analyses of such complex structures, the level of structural detail obtained was only possible due to a combination of MEM recycling and Rietveld analysis.

Experimental Section

The sample, of nominal composition Ca_4C_{60}, was prepared by solid-state reaction of small Ca particles with C_{60}. The Ca particles were obtained by dissolving Ca metal in liquid ammonia at 210 K and then by removing the ammonia under dynamic vacuum at 10^{-6} Torr at 423 K for 24 h. The reaction mixture was annealed in a Ta tube under a vacuum of 10^{-6} Torr at 823 K for 10 days. The sample was then ground in a glovebox and annealed again at 823 K for 1 day. The sample was introduced into a 0.7-mm capillary in the glovebox. The

(11) Collins, D. M. *Nature* **1982**, *298*, 49−51.
(12) Sakata, M.; Uno, T.; Takata, M.; Mori, R. *Acta Crystallogr., Sect. B: Struct. Sci.* **1992**, *48*, 591−598.
(13) Collins, D. M. *Z. Naturforsch., A: Phys. Sci.* **1993**, *48*, 68−74.
(14) Takata, M.; Nishibori, E.; Sakata, M. *Z. Kristallogr.* **2001**, *216*, 71−86.
(15) Izumi, F.; Ikeda, T.; Sasaki, T.; Kumazawa, S. *Mol. Cryst. Liq. Cryst.* **2000**, *341*, 1057−1062.
(16) Izumi, F.; Ikeda, T. *A Mat. Sci. Forum* **2000**, *321-3*, 198−203.

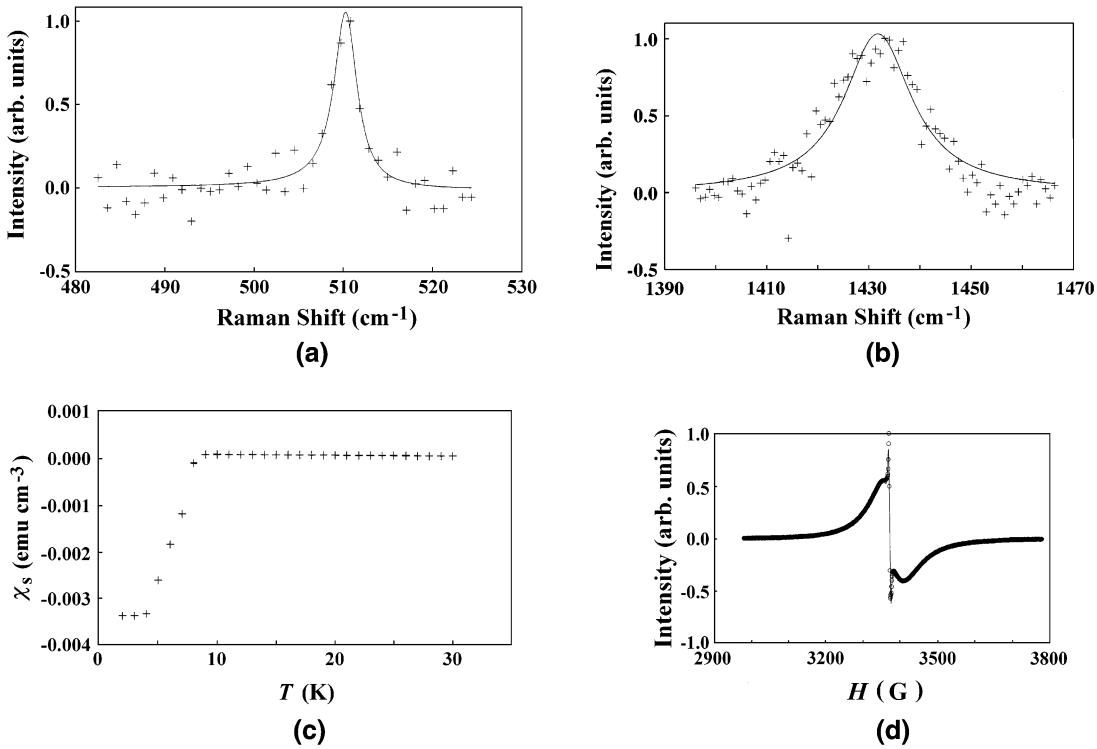

Figure 2. (a) The Raman spectrum of the $A_g(1)$ mode of $Ca_{3.01}C_{60}$. (b) The Raman spectrum of the $A_g(2)$ mode of $Ca_{3.01}C_{60}$. (c) The temperature dependence of the zero-field-cooled susceptibility of $Ca_{3.01}C_{60}$ demonstrates the onset of superconductivity at 9 K. (d) The EPR spectrum of $Ca_{3.01}C_{60}$ consists of three distinct resonances as described in the text.

X-ray powder diffraction pattern was measured at 298 K with synchrotron radiation (λ = 0.8517 Å) at BL-1B of Photon Factory at High Energy Acceleration Research Organization (KEK-PF). The diffraction data were collected with a cylindrical imaging plate with a collection time of 1200 s. Rietveld analysis was performed with the GSAS and RIETAN codes. The subsequent MEM charge density analysis was carried out using the MEED program developed by Sakata and coworkers.[14,17−21]

Raman spectra were recorded at 298 K with He−Ne laser excitation of 632.8 nm on a Confocal Raman Imaging LabRam system (Jovan-Ybon). Magnetic measurements were performed in a 5G measuring field with a Quantum Design MPMS2 SQUID magnetometer. EPR data were recorded at 300 K with a Bruker ESP300 ESR spectrometer. The sample was introduced into a 4-mm quartz tube in the glovebox and the tube sealed under 10^{-6} Torr.

Results

The $A_g(2)$ and $A_g(1)$ Raman modes of the fulleride anion were observed at 1432 and 510 cm^{-1}, respectively (Figure 2a,b). The $A_g(2)$ frequency is downshifted by 36 cm^{-1} from pristine C_{60}, which is entirely consistent with the −6 charge derived from the crystallographically refined composition. The superconducting transition was observed at 9 K from the temperature dependence of the static susceptibility (Figure 2c), with a superconducting volume fraction of 4.25% at 2 K. This small volume fraction is typical of that previously found for calcium fulleride systems and complicates attempts to unambiguously assign the superconducting phase composition. This paper therefore concentrates on crystallographic characterization. The EPR spectrum (Figure 2d) of this phase is composed of the conduction electron resonance at g = 1.9981 and ΔH_{pp} = 88 G (which obeys the Elliot relation for the temperature dependence of the relaxation rate and accounts for 83% of the observed intensity) and two further peaks (g = 2.0056, ΔH_{pp} = 4.6 G, 1% intensity and g = 2.0058, ΔH_{pp} = 37 G, 16% intensity).

LeBail analyses of the synchrotron X-ray data did not distinguish between the $Pa\bar{3}$ and *Pbca* space groups, and subsequent analysis was therefore carried out in $Pa\bar{3}$. The doubling of the unit cell in each direction produces 32 C_{60} molecules occupying the 4a and 4 b$\bar{3}$ symmetry positions and the 24d general position at $^1/_4{}^1/_4 0$ (Figure 1b) as outlined in more detail in the discussion section. These site symmetries restrict the 4a and 4b site anions to rotation about 3-fold axes passing through hexagonal faces aligned with the symmetry directions, whereas there is no symmetry constraint on the orientational setting of the anions occupying the general positions. Given the potential complexity of the structure with cations partially occupying multiple displaced sites and differing anion orientations for each of the three inequivalent anion sets, an initial model was constructed from rigid body C_{60} anions with setting angles generated by 38° rotations about local [111] axes as found for $Yb_{2.75}C_{60}$. The tetrahedral site locations and occupancies were taken from previous literature models, and a cube of cations occupying octahedral site centers with equal occupancy was used. It should be noted that structural analysis of Ca_xC_{60} is more sensitive to correct description of the anion orientations than in the lanthanide

(17) Sakata, M.; Mori, R.; Kumazawa, S.; Takata, M.; Toraya, H. *J. Appl. Crystallogr.* **1990**, *23*, 526−534.
(18) Sakata, M.; Sato, M. *Acta Crystallogr., Sect. A: Found. Crystallogr.* **1990**, *46*, 263−270.
(19) Sakata, M.; Takata, M. *High Pressure Res.* **1996**, *14*, 327−333.
(20) Takata, M.; Umeda, B.; Nishibori, E.; Sakata, M.; Saito, Y.; Ohno, M.; Shinohara, H. *Nature* **1995**, *377*, 6544.
(21) Kumazawa, S.; Takata, M.; Sakata, M. *Acta Crystallogr., Sect. A: Found. Crystallogr.* **1995**, *51*, 47−53.

fulleride cases due to the smaller electron density of the cations.

The initial refinements involved rotation of the C_{60} anions about all the symmetry-allowed axes (the unique 3-fold axis in the case of the $\bar{3}$ symmetry 4a and 4b positions and three orthogonal axes in the case of the 24d anions) and refinement of the positions and occupancies of the cations. These analyses revealed a strong correlation between these variables, which particularly strongly affected the refined occupancies and positions of the minority cube corner positions on the octahedral sites. To produce a structural model uncorrelated with the initial assumptions concerning cation locations and anion orientations, the observed scattering density was analyzed with the maximum entropy method implemented in the MEED code of Sakata and co-workers.[14,17−19] The aim of these analyses was to identify independently the occupied cation positions. The maximum entropy maps were constructed using an array of 100 × 100 × 100 voxels to describe the electron density, dividing each axis into 0.28-Å steps. The integrated intensities and initial phases (derived from the final Rietveld model) of the 1492 observed reflections at angles below 44.6° 2θ were used.

These initial maximum entropy F_{obs} Fourier maps allowed the location of the three T sites and two 100% occupied corners of the cation cubes initially placed on the O sites, together with a variety of other sites of lower electron density, which were possibly occupied. To minimize the biasing effect of the initial model on the maximum entropy electron density maps, the electron density thus calculated was recycled via a REMEDY analysis until no further improvement in R_I was observed (R_I decreased from 11.21% using the scattering density originally obtained from the Rietveld analysis to 4.43% from the optimized scattering density derived from the REMEDY cycles).

Figure 3 demonstrates the utility of the MEED maps in differentiating between fully occupied, partially occupied, and empty sites. The resulting electron density map contained the three symmetry-independent C_{60} anions and nine peaks which could not be assigned as part of the molecular structure of C_{60}. The geometries of the anions generated by assigning the carbon atoms from the MEED peaks were surprisingly regular given the limited (1.1 Å) resolution of the data, but not sufficiently chemically sensible to allow their use in subsequent Rietveld analysis (even the synchrotron data set is underdetermined for the analysis of 80 C positions), and therefore rigid-body C_{60} anions were used in the final refinements. The MEM-derived cation positions were initially fixed, and their occupancies together with the rigid body setting angles were refined. To avoid local minima, the anion setting angles were started in orientations separated by 30° rotations about each of the five axes. This procedure confirmed the validity of the cation positions identified by the MEED analysis and revealed that the setting angle of the ($^1/_4$ $^1/_4$ 0) anions differed significantly from the original position, χ^2 reducing from 6 to below 3 upon this adjustment. The final refinement cycles involved no constraints on the positions or occupancies of any of the cation positions in the model, full refinement of symmetry-allowed anion setting angles, and refinement of

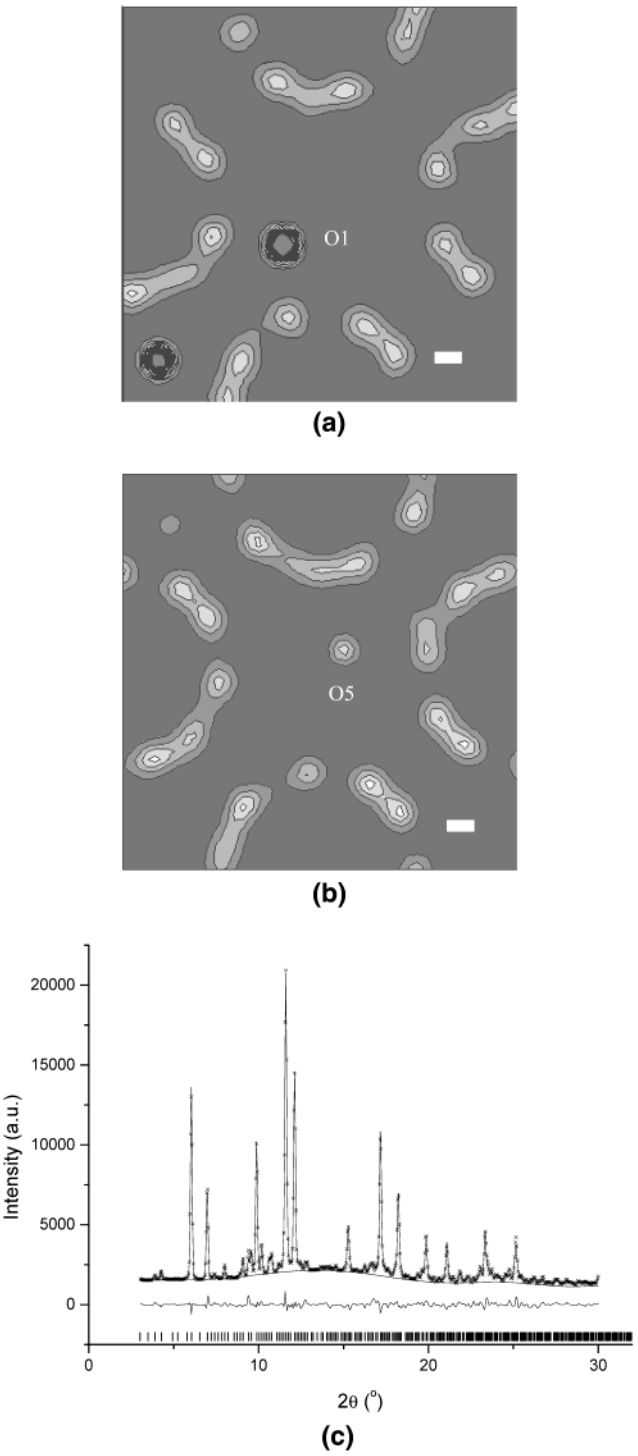

Figure 3. MEED electron density map ($0 \le x \le {}^1/_2$ $0 \le y \le {}^1/_2$) at (a) $z = 0.20$ and (b) $z = 0.28$, clearly showing the fully occupied O1 site in (a) and the partially occupied O5 in (b). It can be clearly seen that there is no significant electron density in the corners of the cube not occupied by O1 or O5. Contours are marked at intervals of 1 e Å^{-3} and the scale bar marked is 1 Å. (c) The profile fit to the final REMEDY cycles corresponding to the maximum entropy electron density maps shown in (a) and (b) above. $\chi^2 = 6.51$, $R(F^2) = 4.5\%$, $R_w = 5.10\%$, $a = 27.908(22)$ Å.

three separate isotropic displacement parameters (to describe all the carbon atoms in all three anions and (separately) the tetrahedral and octahedral site cations—this first assumption is probably incorrect as signaled by the small negative value refined for the C atoms, but

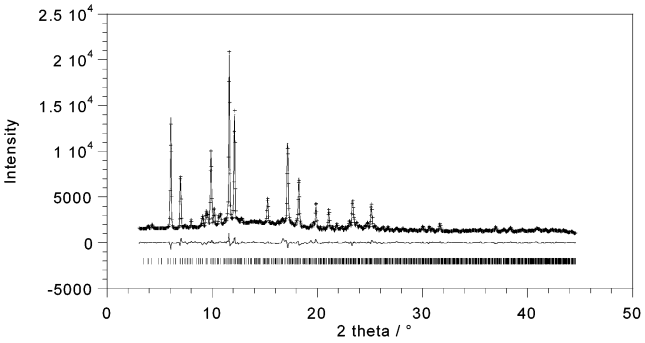

Figure 4. Rietveld refinement of synchrotron X-ray powder diffraction data collected on $Ca_{3.01(2)}C_{60}$ with the refined parameters shown in Table 1. The observed data are shown as points, the calculated model is the solid line, and the difference is plotted below. The tick marks indicate the positions of the allowed Bragg reflections. $\chi^2 = 3.21$, $R(F^2) = 5.69\%$, $R_w = 3.33\%$, $a = 27.907(1)$ Å, $V = 21733.0(2)$ Å^3.

Table 1. Refined Ca Positions in $Ca_{3.01(2)}C_{60}$[a]

	x	*y*	*z*	100 U_{iso}/Å^2	position	occupancy
CaT2	0.6159(8)	0.1402(7)	0.1130(8)	4.2(4)	24d	1.0000
CaT3	0.8711(7)	0.1335(7)	0.1227(10)	4.2(4)	24d	1.0000
CaT4	0.8818(8)	0.3818(8)	0.1182(8)	4.2(4)	8c	1.0000
CaO1	0.0558(7)	0.2066(7)	0.0461(7)	1.6(5)	24d	1.0000
CaO2	0.199(3)	0.199(3)	0.199(3)	1.6(5)	8c	1.0000
CaO5	0.8050(8)	0.0534(8)	0.0540(8)	1.6(4)	24d	0.22(2)
CaO12	0.277(1)	0.277(1)	0.277(1)	1.6(5)	8c	0.38(3)

[a] The idealized coordinates of the unoccupied cube corners are given in Table S2.

the data do not permit a more rigorous analysis). The refined composition is $Ca_{3.01(2)}C_{60}$. The final refinement is shown in Figure 4 and the refined cation parameters are shown in Table 1, with the anion carbon positions given in Table S1 (see Supporting Information).

Discussion

The introduction of eight ordered T site vacancies (on the 8c ($^1/_8$, $^1/_8$, $^1/_8$) and equivalent positions in the doubled cell) alters the symmetry of both the C_{60} anions and the O sites and produces significant relaxation of their local environments. As the supercell contains eight fcc subcells, there is one vacancy within the cube described by the tetrahedral sites within each subcell (Figure 1a). This generates three symmetry-inequivalent classes of tetrahedral sites within each cube—one site on the body diagonal opposite the vacancy and two sets of three equivalent sites related by the one remaining 3-fold axis (connecting the vacancy and the T site lying on the same body diagonal) within the cube. The single vacancy per cube of T sites defines local 3-fold axes, which also generate inequivalencies between the 32 octahedral sites in the 8-fold supercell. The eight O sites in the centers of the cubes of tetrahedral sites lie on the 3-fold axes remaining after the T vacancy creation, occupying 8c xxx positions, whereas the other 24 O sites have no point symmetry (Figure 1b). Although structural analysis reveals that the centers of these sites are unoccupied in Ca_xC_{60}, their point symmetries play an important role in systematizing the resulting structure.

The structural chemistry of sodium with C_{60}[9,10] and potassium with C_{84}[22] contains cubes and tetrahedra

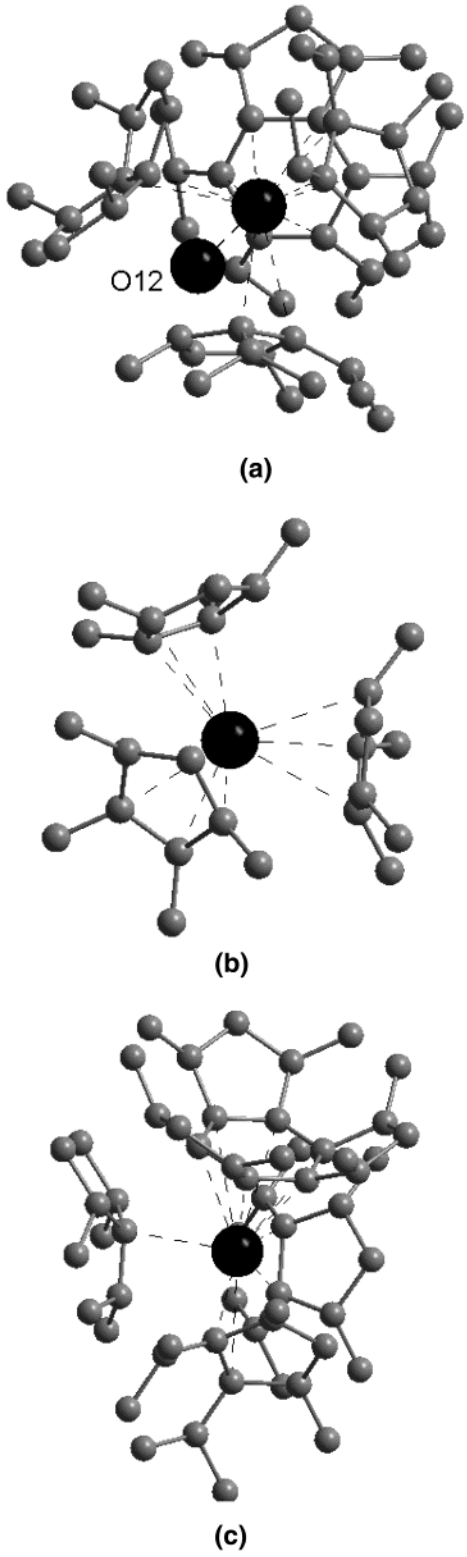

Figure 5. Near-neighbor environments of the three fully occupied tetrahedral sites in Ca_xC_{60}. (a) The T4 cation is displaced 0.32 Å away from the site center to maximize its distance from the O12 cation, displaced from the center of a neighboring O site. (b) The T2 site is displaced by 0.6 Å from the site center and thus has only three near-neighbor anions, making Ca...C contacts less than 3 Å. (c) The T3 environment is less symmetrical than the two other occupied T sites, with three distinct coordination modes.

occupying the octahedral site, formed by cation displacements away from the octahedral site center along

Table 2. Ca...C Contacts (Å): Distances Are Given as Groups Corresponding to Carbon Atoms Derived from Specific C_{60} Anions—Normal Font Is 4a, Bold Is 4b, and *Italic* Is 24d

CaO1_C11	2.97(2)	*CaO5_C37*	*2.8(1)*	*CaT3_C56*	*2.963(27)*
CaO1_C13	2.92(2)	*CaO5_C61*	*2.75(9)*	*CaT3_C61*	*2.836(23)*
		CaO5_C67	*2.41(9)*		
CaO1_C40	*2.65(2)*			*CaT3_C36*	*2.971(28)*
CaO1_C52	*2.63(2)*	*CaO5_C42*	*2.86(9)*	*CaT3_C42*	*2.976(29)*
CaO1_C70	*2.76(2)*	**CaO5_C54**	**2.77(9)**	*CaT3_C54*	*2.974(28)*
CaO1_C81	*2.81(3)*	*CaO5_C86*	*2.9(1)*	*CaT3_C60*	*2.960(28)*
CaO1_C87	*2.73(2)*			*CaT3_C84*	*2.965(29)*
		CaT2_C22	**2.85(3)**	*CaT3_C90*	*2.961(29)*
CaO1_C89	*2.87(2)*	**CaT2_C24**	**3.00(4)**		
CaO1_C69	*2.95(2)*	**CaT2_C27**	**2.80(3)**	**CaT4_C23**	**2.845(35) ×3**
CaO1_C83	*2.96(2)*	**CaT2_C29**	**2.94(5)**	**CaT4_C28**	**2.843(34) ×3**
CaO1_C51	*2.80(2)*				
CaO1_C39	*2.86(2)*	*CaT2_C68*	*2.73(2)*	CaT4_C71	2.79(3) ×3
		CaT2_C38	*2.85(2)*	CaT4_C79	2.81(2) ×3
CaO2_C33	*2.69(2) ×3*	*CaT2_C82*	*2.85(2)*		
CaO2_C45	*2.89(1) ×3*				
CaO2_C57	*2.67(2) ×3*	*CaT2_C58*	*2.85(3)*		
CaO2_C62	*2.88(1) ×3*	*CaT2_C66*	*2.65(2)*		
		CaT2_C78	*2.78(2)*		
CaO12_C77	*2.870(21) ×3*				
		CaT3_C17	2.82(3)		
CaO5_C15	2.72(9)				
CaO5_C19	3.0(1)	*CaT3_C59*	*2.857(25)*		
CaO5_C20	2.3(1)	*CaT3_C64*	*2.780(25)*		

the four equivalent 3-fold axes. As the T vacancy-ordered $Yb_{2.75}C_{60}$ phase displays significant displacements of O site cations along similar directions,[6] cation occupancy of corners of cubes centered on O sites needs to be considered. The 8c 3-fold symmetric set of O sites are described by 64 cube corner positions, two 8c positions corresponding to positive or negative displacements along the 3-fold axis (O2 and O12), and two 24d sets which correspond to the other six vertexes of the cube which divide into two sets of 3-fold related atoms on each O site (O10, O11). The eight cube corner positions on the 24d general position O sites each correspond to a separate 24d site as each cube corner is symmetry-unique. Thus, a total of 12 positions, only two of which are symmetry-constrained to lie on the 3-fold axes, are required to describe the cation cubes which may occupy the O sites, and these sites are listed in Table S2 (see Supporting Information). Relaxation of cube corner sites on the 24d O positions away from the putative 3-fold axes is allowed in our analysis.

The T site vacancy ordering also differentiates between the 32 C_{60} anions in the supercell. The C_{60} anions at 0,0,0 (4a) and $^1/_2,^1/_2,^1/_2$ (4b) are located on 3-fold axes whereas the remaining 24 form a set on general positions. The T vacancies have three general position C_{60}'s and one from the 4a (000) set as neighbors, and this results in the 4b C_{60} positions at the center of the supercell having no T vacancy near neighbors—the 4a 000 sites have two and the 24d C_{60}'s have one. The 3-fold axes remaining after the T vacancy ordering therefore define the orientational degrees of freedom of the C_{60}^{n-} anions: the distinct 4a and 4b sets are restricted to rotations about the 3-fold axes passing through hexagonal faces of the anions, whereas the 24 anions located on general positions do not have any restrictions on their orientational setting. These differing anion symmetries are explicitly included in our refinements through the rigid body rotation axes used, and thus the derived cation–anion contacts are not restricted by unnecessary assumptions about rotations around 3-fold axes.

The three sets of T sites are fully occupied, and their location with respect to the site centers is determined by the point symmetry (no extra assumptions being made, for example, concerning displacements along local 3-fold axes) and the occupancy of neighboring octahedral sites. The 8c symmetry T4 site, on the 3-fold axis passing through the near-neighbor vacancy, is displaced away from the site center along the 3-fold axis toward its C_{60} neighbor from the 4a set and away from the three 24d neighbors to maximize its distance from the O12 cation occupying the corner of a cube centered on a neighboring O site (Figure 5a). This cation displacement toward the 4a anion is along the 3-fold axis toward a hexagonal face, which permits approximately equidistant near-neighbor Ca...C contacts to all four neighboring anions, as the three equivalent contacts to the 24d anions are to 6:5 bonds on a pentagonal face (Table 2). The partial occupancy of the O12 site is thus driven by the ability of the T4 cation to relax toward the six-ring of a neighboring anion, explaining why this cube vertex, of seven other possible cube vertexes, on the 8c O sites is occupied.

The T2 site has a lower coordination number than T4 as the enhanced displacement from the site center results in close contacts of only three anions. Although these anions are symmetry-inequivalent, the contact distances and modes are similar, involving three atoms of a pentagonal face in each case (Figure 5b).

The T3 site displacement (Figure 5c) is similar to that of T4, being toward an anion which coordinates via a hexagonal face. The three other anions coordinate via two 6:5 bonds and a single carbon atom, the latter being the most distant from the cation. This demonstrates the variety of coordination modes produced by the T vacancy ordering and resulting cation displacements.

As previously demonstrated for $Yb_{2.75}C_{60}$,[6] the relaxation of the O site cations from the site centers is much greater than that for the T cations. The occupancy of

(22) Allen, K. M.; Dennis, T. J. S.; Rosseinsky, M. J.; Shinohara, H. *J. Am. Chem. Soc.* **1998**, *120*, 6681–6689.

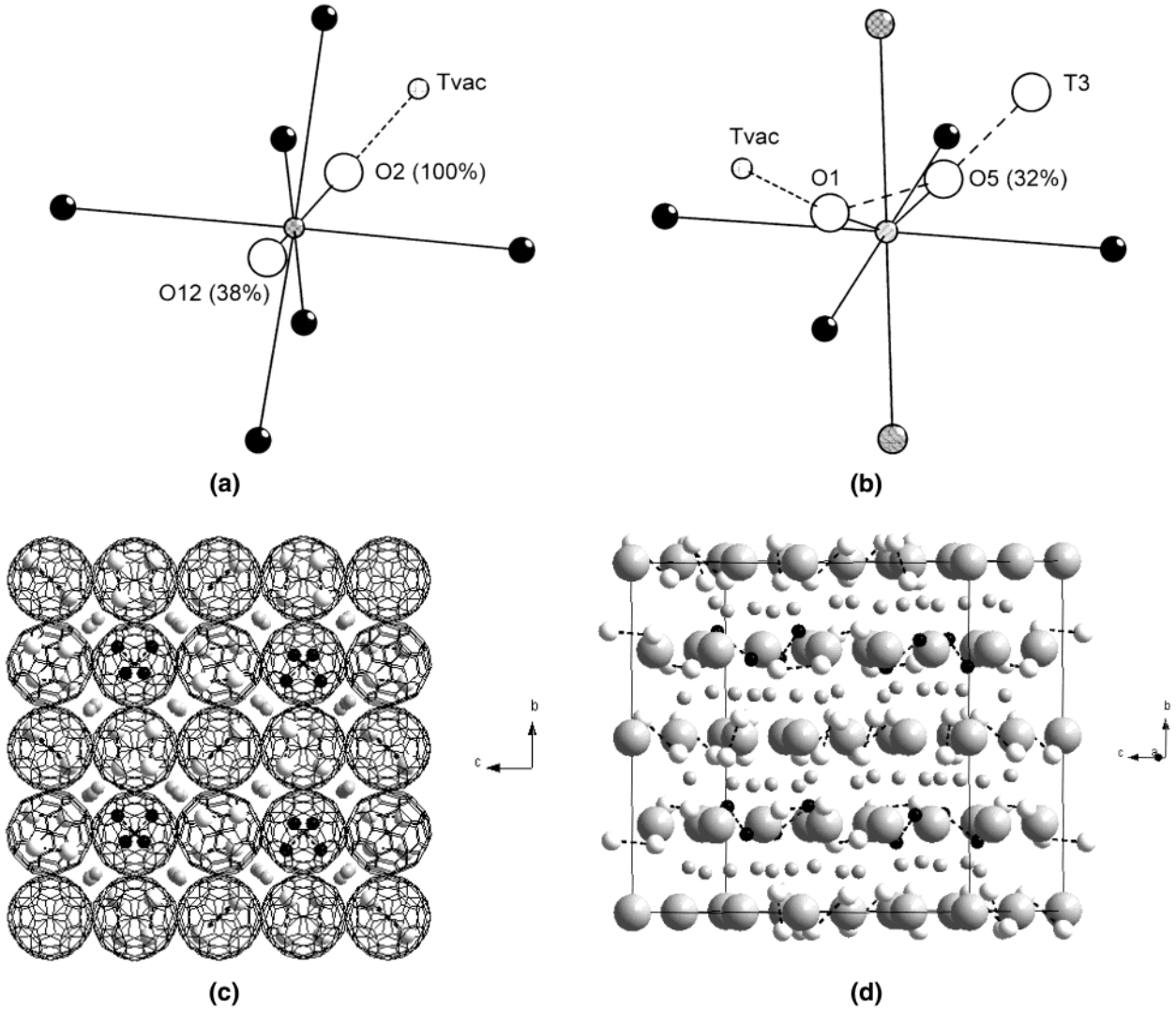

Figure 6. The occupancy of the two symmetry-inequivalent octahedral sites in Ca_3C_{60}. (a) The 8c sites lie at the centers of the cubes of T sites in the subcell and consequently retain one 3-fold axis in the supercell. Both cations occupying the site lie on this axis. The center of the 8c site is represented by a hatched sphere; the two Ca cations (unshaded) occupying the site are displaced in opposite directions along the 3-fold axis, and the six 24d site C_{60} anions are represented as black spheres. The near-neighbor T vacancy is shown as a quartered sphere. (b) Nearest-neighbor C_{60} anions and occupancy of the 24d set of octahedral sites. Ca cations are unshaded, the 24d C_{60} anions are black spheres, the 4a C_{60} anions are light spheres, and the 4b C_{60} anions are hatched gray. The T vacancy is represented as a quartered sphere. Note that both the O1 and O5 cations occupying this site coordinate to the 4a C_{60} anion. The refined structure of $Ca_{3.01}C_{60}$ (c) with the fulleride anions represented as molecules. The Ca cations occupying the T sites are small gray spheres whereas those on the O sites are larger dark (8c sites, occupied by O2 and O12 cations) and light (24d sites, occupied by O1 and O5 cations) spheres, with the intercation contacts on the O sites represented as broken solid lines. The refined structure of $Ca_{3.01}C_{60}$ (d) with the fulleride anions represented as spheres, allowing a clearer view of the intercation contacts on the O sites: the representation of the cations is the same as in (a) above.

the cubes centered on the two sets of symmetry-inequivalent O sites can best be considered by examining the cation distribution around the site centers. The 8c O sites located on 3-fold axes are surrounded by six general position anions, and in each case only two of the four possible cube corner sites are occupied (corresponding to six of the eight corners of the cube being empty), with the O2 and O12 sites located on the 3-fold axes being 100% and 38% occupied, respectively—the 180° angle between these sites maximizes the intercation distance for a given amplitude of off-center displacement. The fully occupied O2 site is displaced away from the site center by 2.47 Å toward the tetrahedral site vacancy: the displacement (Figure 6a) of O12 from the site center is necessarily smaller (1.31 Å) as it moves the cation toward the fully occupied T4 site (this would be the case for any cube corner site other than O2), producing 5.01(7) Å contact to T4, compared with the O2−T vacancy distance of 3.62 Å (Figure 6a). The O2−O12 distance is 3.78(7) Å, although this is an average of the O2 position over the 62% of 8c octahedral sites in which O12 is not occupied and the 38% of sites in which it is, and the local intercation separation is likely to be larger.

The large-amplitude static displacement of the O2 site (Figure 7a) from the 8c O site center gives three symmetry-equivalent near-neighbor anions which coordinate with five-rings. (The O2 cation is located close to the centroids of the pentagons as four of the five carbons have Ca...C contacts of <3 Å.) The O12 cations are located over a 6:5 bond of the other three anions constituting the 8c O site (Figure 7b). The other

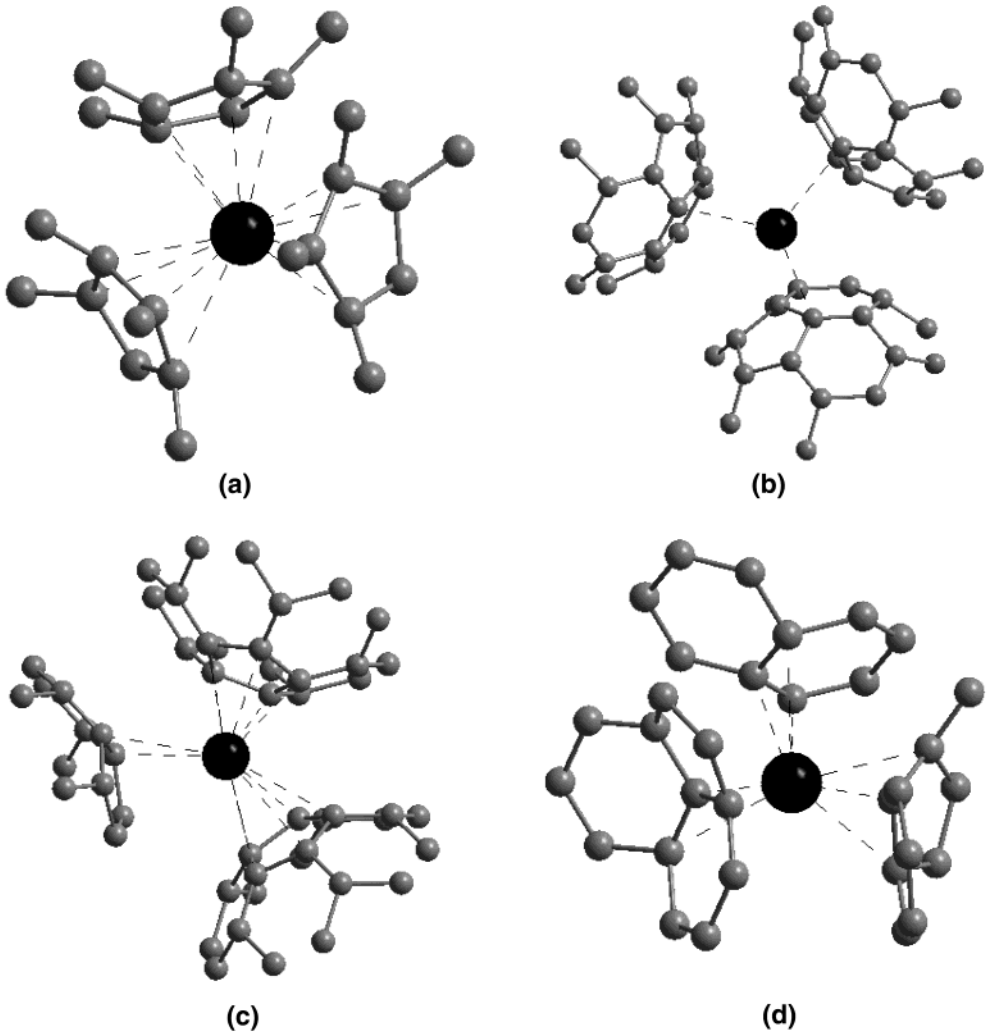

Figure 7. Near-neighbor environments of the calcium cations multiply occupying the O sites in $Ca_{3.01}C60$. (a) Ca...C contacts on the fully occupied O2 cube corner site, displaced along the 3-fold axis 2.47A from the center of the 8c octahedral site. The cation makes three equivalent contacts to 24d C60 anions, lying near the centroid of a five-membered ring in each case. (b) The O12 cube corner site, displaced from the 8c center in the opposite sense to O2. (c) The O1 cube corner is fully occupied on the 24d set of O sites. It is closest to two 24d anions which each coordinate via a five-ring, whereas the more distant 4a C60 binds the cation via a 6:5 bond. (d) The O5 site is 22% occupied on the 24d O sites. It is coordinated to a six-ring and a 6:6 bond as well as a five-ring.

cube corner positions on this set of O sites have no scattering density in either the MEED or Rietveld analyses.

The cations occupying the cube corner positions on the other 24 O sites are not constrained by symmetry to lie on 3-fold axes. As in the 8c case, only two (O1 and O5) of the eight cube corner sites are occupied (Figure 6b), and the fully occupied O1 site is displaced 2.38 Å from the site center to be 3.67 Å from the T vacancy (Figure 7c). The partially (22(2)%) occupied O5 site is displaced 2.37 Å from center toward the fully occupied T3 (T3...O5 3.70 Å, similar to the on-O site O2−O12 contact on the 8c set of O sites) with the intra-O site O1−O5 contact being 4.15(7) Å. The displacement from the site center of the minority cation is larger than that found for the 8c O sites because the two cations do not occupy the same body diagonal, the intercation distance corresponding to the edge rather than to the body or face diagonal of the cube. As this is the closest inter-vertex contact possible on a partly decorated cube, the co-occupancy of these positions in 22(2)% of the 24d O sites may be related to favorable interactions with the 4a C_{60} anion which both O1 and O5 have as a near neighbor (Figure 6b). Neither occupied site interacts with the 4b C_{60}, whereas each interacts with a pair of the four 24d anions, completing this set of O sites.

The fully occupied O1 site (Figure 7c) is closest to one of the 24d anions and located close to a pentagon centroid; the coordination to the second 24d anion is similar, while the 4a anion also directs a five-ring toward the C_{60} but coordinates closely only via a 6:5 bond, as demonstrated by the distances in Table 2. The cation is displaced by 0.3 Å from the 3-fold axis which it would lie on in an ideal octahedral site.

O5 coordinates to the shared 4a anion via its 6:6 bond (Figure 7d), a coordination mode not found for the other cation sites, whereas the two 24d anions not binding to O1 coordinate via three atoms of a five-ring. It is displaced by 0.2 Å from the 3-fold axis, on which it would lie in an ideal octahedral site.

The octahedral sites thus divide into two symmetry-inequivalent sets which are both partially multiply occupied. The position of the fully occupied species on both sites is determined by displacement toward the

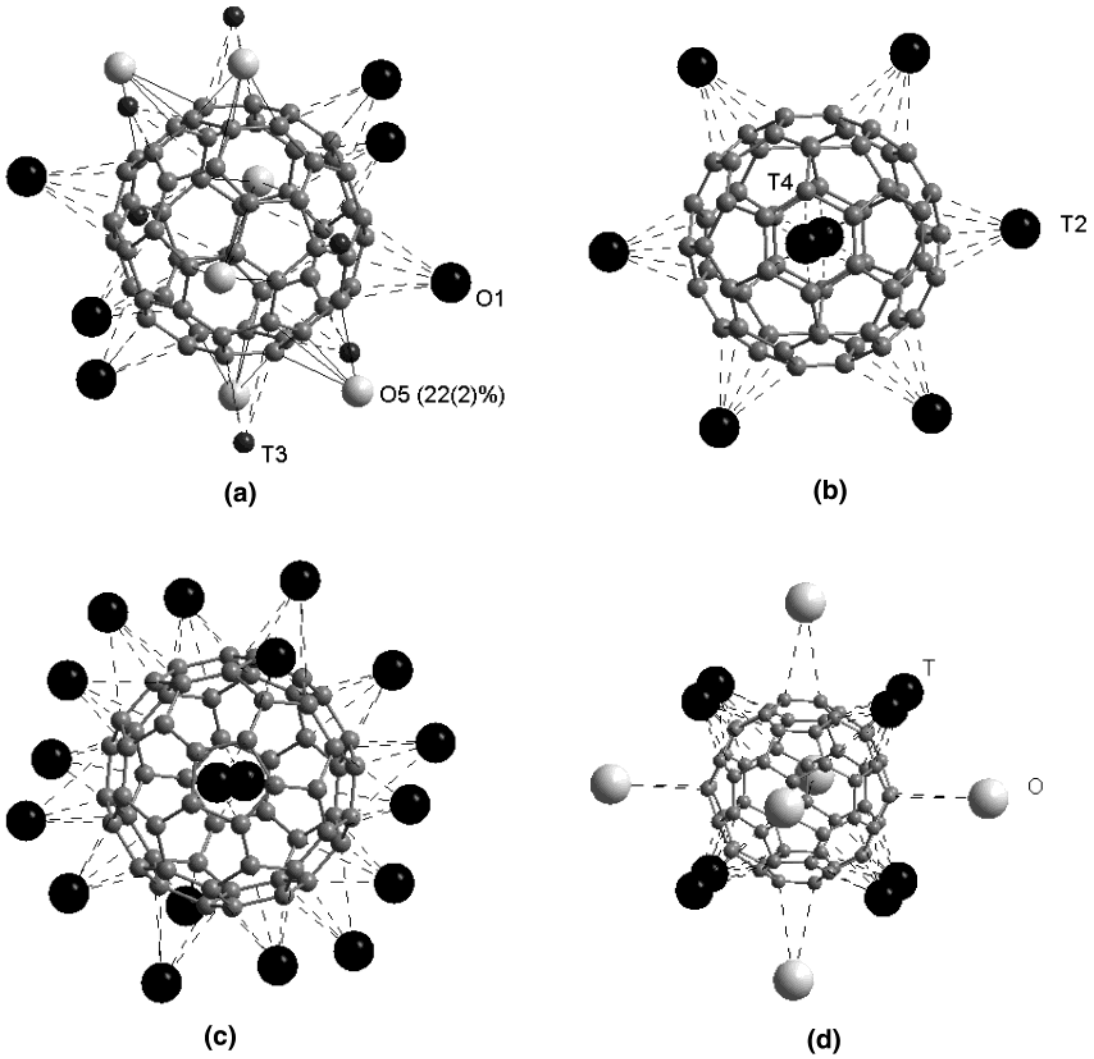

Figure 8. (a) The 4a anions have a cation coordinating to each five−ring (six T3 (small gray spheres), six O1 (black)), and six 22% occupied O5 positions (light gray) coordinating to a 6:6 bond. (b) The 4b anions are surrounded by a cube of cations, but only the T4 sites lying over the six-membered rings are fully occupied. (c) The 24d anions have a noncentric cation environment. The fully occupied O1 cation lies over the centers of two of the five-rings whereas the T3 site lies over two of the five- and one of the six-rings. O5 (22(2)%) lies over one five-ring and one six-ring center whereas the other partially occupied site (O12) makes contact to a 6:5 junction. T2 lies over two pentagon centers and a 6:5 bond. T4 also lies over a five-ring center. The O2 site lies over a pentagon centroid. As for the 4a anions, all 12 pentagonal rings are coordinated by calcium cations and six hexagonal faces. Nine five-ring centers, two 6:5 bonds, and two six-rings are coordinated by cations, with the two partially occupied cation sites both binding to pentagons, which would otherwise be uncoordinated. (d) The anion environment in the 14-Å cell fcc. A_3C_{60} structures (two equivalent anion orientations related by 90° rotation about 6:6 bonds are present, of which only one is shown), showing the eight O and six T neighbors.

octahedral face closest to the tetrahedral site vacancy. The intercalcium distances produced by the multiple occupancy are similar in both cases but due to contacts to cations occupying the same site (8c sites) or a neighboring T site (24d sites). The multiple occupacny of the octahedral sites within the supercell is depicted in Figure 6c,d.

Despite the total Ca concentration being greater than 3, and the phase forming part of a solid solution series of Ca_xC_{60} phases, the T vacancy ordering found in the line phase $Yb_{2.75}C_{60}$ remains the decisive factor in the structural chemistry. The two symmetry-inequivalent O sites, which feature substantial cation relaxations from the site center driven by the T site vacancies and the need to optimize the Ca...C interactions, have different minority cation sites populated. The displacement of the majority site allows population of less favored cube corner positions, and the Ca...C and Ca...Ca interactions possible on each site determine which are occupied. The power of the MEED/REMEDY analysis is demonstrated by the almost exact agreement between the refined calcium concentration and the t_{1u} orbital occupancy derived from the $A_g(2)$ mode frequency, which independently demonstrates the correctness of the refined structure.

The mean radii of the anions with 3-fold symmetry (4a and 4b positions) and on general positions refine to have the same value within error, and these values were fixed in the final refinements. The refinements are not sensitive to any differences in charge transfer to the different sets of anions.

The 4a anions (Figure 8a) coordinate to the partially occupied O5 site via a 6:6 bond—the carbon atom most closely interacting with this cation forms part of the five-ring bound to T3, which is displaced to coordinate to the 6:5 bond most distant from the carbon bound to O5.

Six of the pentagonal faces connect to T3 in this way. The remaining six pentagonal faces are coordinated to the fully occupied O1 cation which, in contrast to O5, is located close to the pentagon centroid as there is no need for displacement to accommodate other cations in this case.

The 4b anions are undercoordinated (Figure 8b), with a rhombohedrally distorted cubic environment formed by two contacts to the T4 site, which lies over two diametrically opposed six rings and six to the T2 sites, which lie over six of the pentagonal faces of the 4b anion.

The 24d anions (Figure 8c) have a noncentric environment in which 11 of the 12 five-membered rings are coordinated to cations—two of these rings are only able to bind to cations that partially occupy the octahedral sites.

The above distinct anion orientations need to be compared with the C_{60}^{3-} environment in K_3C_{60}, where none of the neighboring eight tetrahedral or six octahedral sites are bound to a pentagonal face. The octahedral sites' closest approach is to a 6:6 bond whereas the tetrahedral sites are located over eight hexagonal faces directed along the ⟨111⟩ directions—the cation displacements in $Ca_{3.01(2)}C_{60}$ combine with the anion orientation to allow closer anion−cation contact by allowing more five-rings to bind with the cations. This allows an increase in the number of near-neighbor cations from 14 to 18 in the case of the 4a and 24d anions, balanced by the reduced coordination of the 4b anions, which only have eight neighbors.

Conclusion

The tetrahedral cation vacancy ordering in $Ca_{3.01(3)}C_{60}$ dominates the structural chemistry as it does in $Yb_{2.75}C_{60}$. The maximum entropy analysis performed here allows the detailed examination of this ordering on the occupancy of the octahedral sites and the orientational setting angles of the three inequivalent sets of fulleride anions within the unit cell. The anions coordinate to the cations largely but not exclusively via their pentagonal faces, and a variety of local bonding geometries are revealed. The site center displacements of the octahedral cations allows much closer contacts than are found in alkali metal fullerides, suggestive of enhanced metal−anion covalency, and allow sufficient free volume on the O sites for multiple occupancy, as found in the more disordered sodium C_{60} and potassium C_{84} salts previously. The present more highly ordered example allows more insight into the factors locally controlling cation location and anion orientation—the closest cation−cation contacts may be either on the same O site or with neighboring T sites and can drive correlated displacements of the T site cations along directions selected by the orientational ordering of the anions. The local cation configurations on the multiply occupied octahedral sites in Na_xC_{60} and K_xC_{84} are therefore not straightforward for deducing from the overall occupancies and the proximity of the cube vertexes on the O site. The maximum entropy method proves itself to be a powerful technique for resolving complex crystallographic problems in these fulleride superstructures where the influence of anion orientational order and disordered cation site occupancy are hard to deconvolute using conventional least-squares and Fourier recycling analysis. In the present case, the specific advantages are the ability to refine the orientationally ordered structure in cubic rather than orthorhombic symmetry without making assumptions about the occupancy of the minority cation site positions or occupancies, developing a clear picture of the influence of the T site vacancy ordering which dominates the gross features of the structure, on local structural detail.

Acknowledgment. We thank the UK EPSRC for support under GR/M04006. The X-ray diffraction measurements were performed under the auspices of KEK-PF (Grant No. 2001G-058). Y.K. acknoweldges the Japanese Ministry of Education, Science, Sports and Culture for their support of his visit to the United Kingdom.

Supporting Information Available: Tables of carbon positions and the reduction in symmetry of the calcium sites. This material is available free of charge via the Internet at http://pubs.acs.org.

CM020171Y